A Control–Oriented Model of Underwater Snake Robots

E. Kelasidi, K. Y. Pettersen and J. T. Gravdahl

Abstract— **In this paper we consider swimming underwater snake robots that are fully immersed in water and moving in a virtual horizontal plane. The main objective of the paper is to develop a model that is well suited for control design and stability analysis for swimming snake robots. The proposed model is notably less complex than the existing models, while significant parameters such as added mass effects, linear drag forces, torques due to the added mass and linear drag forces, are all taken into account in the modeling. An extensive analysis of a previously proposed complex model of underwater snake robots ([1]) is presented, and from this analysis a set of essential properties that characterize the overall motion of underwater snake robots is derived. The proposed control-oriented modeling approach captures these essential properties, resulting in a less complex model that is well suited for control design, and at the same time has the same essential properties as the complex model. A qualitative validation of this is given by simulations that present a comparison of representative parameters of the complex and the control-oriented models for lateral undulation and eel-like motion.**

I. INTRODUCTION

For centuries, engineers and scientists have gained inspiration from the natural world, while searching for ideal solutions to technical problems. More recently, this process has been termed as biomimetics. Every biological organism living in an aquatic environment, swims by generating a propulsive force through the interaction between the body and the surrounding fluid that is created through a rhythmic body movement. Generally, studies of hyper-redundant mechanisms (HRMs), also known as snake robots, have largely restricted themselves to land-based studies, for which several models for snake robots have been proposed [2]. Empirical and analytic studies of snake locomotion were reported by Gray [3], while, among the first attempts to develop a snake prototype, the work of Hirose [4] is essential. Recently, HRMs are presented that are suited for aquatic propulsion as well [5], [6].

The underlying propulsive force generation mechanism for underwater snake robots has been studied through exploration of the fluid dynamics surrounding the body. In this field, several mathematical models of underwater snake robots have been developed [7], [8], [5], [9], [6], [10], [11], [12]. However, all these models are rather complex and thereby challenging to investigate analytically. In [13], a simplified model of [12] is used to develop a feedback controller that achieves the desired body oscillation, orientation, and locomotion velocity. However, the added mass effects and the torques due to the added mass and drag effects are neglected [13]. In [1], the authors present a modeling approach for underwater snake robots that results in a closed form solution. This modeling approach takes into account both the linear and the nonlinear drag forces (resistive fluid forces), the added mass effect (reactive fluid forces), the fluid moments and current effect.

It is well known that the hydrodynamic forces (fluid forces) induced by the motion of a rigid body in an underwater environment are very complex and highly nonlinear. Therefore, the first contribution of this paper is conducting an extensive analysis of the complex model of a fully immersed underwater snake robot moving in a virtual horizontal plane that was presented in [1]. Based on this analysis the hydrodynamic effects which are essential for the overall behavior of the swimming snake robot are identified. These essential properties form the basis of the second contribution of this paper, which is a control-oriented model of underwater snake robot locomotion aimed at control design and stability analysis purposes. In particular, we develop a control-oriented model that is better suited for analysis and design, while capturing these essential properties.

The development of the control-oriented model is inspired by the modeling approach that was presented in [2], [14] for a land-based snake robot. In these references the authors developed a simplified modeling approach for a planar snake robot describing the body shape dynamics in terms of the translational motion of the links, something which is seen to significantly simplify the equations of motion. Motivated by this work, we will model the underwater snake robot locomotion by the translational motion of each link, in order to exploit that translational motion is generally less complex to model than rotational one.

This paper is organized as follows. Section II gives a brief description of the complex model of underwater snake robots from [1]. This is followed in Section III by an analysis of this model in order to identify the essential properties of underwater snake robot. Section IV presents the development of the control-oriented model of underwater snake robots. In Section V simulation results are presented, comparing the behavior of the complex and the control-oriented models, to validate that the control-oriented model captures the essential properties of swimming snake robot locomotion. Conclusions and suggestions for future research are presented in Section VI.

E. Kelasidi, and K. Y. Pettersen are with the Centre for Autonomous Marine Operations and Systems, Dept. of Engineering Cybernetics at NTNU, NO-7491 Trondheim, Norway. E-mail: {Eleni.Kelasidi,Kristin.Y.Pettersen}@itk.ntnu.no

J. T. Gravdahl is with the Dept. of Engineering Cybernetics at NTNU, NO-7491 Trondheim, Norway. E-mail: Tommy.Gravdahl@itk.ntnu.no

This work was partly supported by the Research Council of Norway through project no. 205622 and its Centres of Excellence funding scheme, project no. 223254-AMOS

II. A COMPLEX MODEL OF THE ROBOT

This section gives a brief description of the complex model of an underwater snake robot moving in a virtual horizontal plane presented in [1]. For further details, please see [1].

A. Kinematics of the underwater snake robot

The underwater snake robot consists of N rigid links of equal length l, interconnected by $N-1$ joints. The mass of each link is uniformly distributed so that the link CM (center of mass) is located at its center point (at length $l/2$ from each side of the joint). All N links have the same mass m and moment of inertia J. The total mass of the snake robot is therefore Nm. The robot is assumed to move in a virtual horizontal plane, fully immersed in water, and has N+2 degrees of freedom (N link angles and the x-y position of the robot). The position of the robot is denoted by $\mathbf{p} = (p_x, p_y) \in \mathbb{R}^2$. The *link angle* of each link $i \in 1,\ldots,N$ of the snake robot is denoted by $\theta_i \in \mathbb{R}$, while the *joint angle* of joint $i \in 1,\ldots,N-1$ is given by $\phi_i = \theta_{i+1} - \theta_i$.

B. Equations of motion of the complex model

In this study we choose to consider a fluid dynamic model where only the added mass effect (reactive fluid forces), linear drag forces (resistive fluid forces) and the fluid torques due to the added mass and drag forces are considered. This leads to simpler equation of motion compared to the full hydrodynamic modeling approach described in [1].

Under anisotropic drag forces, a link has two drag fluid coefficients, c_t and c_n, describing the resistive fluid force in the tangential (along link x axis) and the normal (along link y axis) direction of the link, respectively. The added mass fluid coefficient in the the normal direction of the link is denoted by μ_n. It worth mentioning that the added mass effects are modeled under the assumption that the added mass fluid parameter in the x direction is equal to zero ($\mu_t = 0$), because the added mass of a slender body in longitudinal direction can be neglected compared to the body mass [1]. As shown in [1], the fluid forces on the link i, denoted by $\mathbf{f}_i \in \mathbb{R}^2$, can be written in terms of the link velocity, $\dot{x}_i$ and $\dot{y}_i$, and the link acceleration, $\ddot{x}_i$ and $\ddot{y}_i$, as

$$\mathbf{f}_i = -\begin{bmatrix} F^a_x(\theta_i) & F^a_{xy}(\theta_i) \\ F^a_{xy}(\theta_i) & F^a_y(\theta_i) \end{bmatrix}\begin{bmatrix} \ddot{x}_i \\ \ddot{y}_i \end{bmatrix} - \begin{bmatrix} F^d_x(\theta_i) & F^d_{xy}(\theta_i) \\ F^d_{xy}(\theta_i) & F^d_y(\theta_i) \end{bmatrix}\begin{bmatrix} \dot{x}_i \\ \dot{y}_i \end{bmatrix}, \tag{1}$$

where

$$F^a_x(\theta_i) = \mu_n \sin^2(\theta_i) \tag{2a}$$
$$F^a_{xy}(\theta_i) = -\mu_n \sin\theta_i \cos\theta_i \tag{2b}$$
$$F^a_y(\theta_i) = \mu_n \cos^2(\theta_i) \tag{2c}$$
$$F^d_x(\theta_i) = c_t \cos^2(\theta_i) + c_n \sin^2(\theta_i) \tag{2d}$$
$$F^d_{xy}(\theta_i) = (c_t - c_n)\sin\theta_i \cos\theta_i \tag{2e}$$
$$F^d_y(\theta_i) = c_t \sin^2(\theta_i) + c_n \cos^2(\theta_i) \tag{2f}$$

It is shown in [1] that the equation of the motion of the underwater snake robot in terms of link angles, $\theta \in \mathbb{R}^N$, the position of the CM of the underwater snake robot, $\mathbf{p} = (p_x, p_y) \in \mathbb{R}^2$, and the joint torques, $\mathbf{u} \in \mathbb{R}^{N-1}$, can be written as

$$\ddot{\theta} = g(\theta, \dot{\theta}, \dot{p}_x, \dot{p}_y, \mathbf{u}) \tag{3a}$$
$$Nm\ddot{p}_x = \sum_{i=1}^{N} f_{x,i} \tag{3b}$$
$$Nm\ddot{p}_y = \sum_{i=1}^{N} f_{y,i} \tag{3c}$$

where $g(\theta, \dot{\theta}, \dot{p}_x, \dot{p}_y, \mathbf{u}) \in \mathbb{R}$ is a function of the state vector and the joint torques. The model of the underwater snake locomotion given by (3) is complex from a stability analysis perspective. This complexity is the main motivation behind the control-oriented model developed in Section IV.

III. ANALYSIS OF THE COMPLEX MODEL

In this section, the complex model given by (3) will be analyzed in order to identify a set of properties that characterize the motion of an underwater snake robot. These properties will be used as a basis for the development of a control-oriented model of an underwater snake robot moving in a virtual horizontal plane in Section IV.

A. Analysis of propulsive forces

We begin by deriving an expression for the total force propelling the CM of the underwater snake forward. We choose the inertial coordinate system such that the forward direction of the motion of the underwater snake robot is along the global positive x axis, which means that the propulsive force is simply the sum of all external forces on the robot in the global x direction. Hence, the total force propelling the CM of the robot forward is given (3b) as

$$\begin{aligned} Nm\ddot{p}_x = \sum_{i=1}^{N} f_{x,i} = &-\sum_{i=1}^{N} F^a_x(\theta_i)\ddot{x}_i - \sum_{i=1}^{N} F^a_{xy}(\theta_i)\ddot{y}_i \\ &- \sum_{i=1}^{N} F^d_x(\theta_i)\dot{x}_i - \sum_{i=1}^{N} F^d_{xy}(\theta_i)\dot{y}_i. \end{aligned} \tag{4}$$

From Eq. (4), we can see that the total propulsive force consists of four components: a) first one involving the linear acceleration of the link in the forward direction of motion, $F^a_x(\theta_i)\ddot{x}_i$, b) the second one involving the linear acceleration normal to the direction of motion, $F^a_{xy}(\theta_i)\ddot{y}_i$, c) the third one involving the linear velocity of the link in the forward direction of the motion, $F^d_x(\theta_i)\dot{x}_i$, and d) the last one involving the linear velocity of the link normal to the direction of motion, $F^d_{xy}(\theta_i)\dot{y}_i$. It is easily seen that, due to the minus signs in (4), all the components (2a)-(2f) provide a positive contribution to the propulsive force only if they are negative. Considering that the fluid coefficients due to the drag and the added mass effects are positive, c_t, c_n and μ_n, are always positive, the expressions $F^a_x(\theta_i)$ (2a) and $F^d_x(\theta_i)$ (2d) are also positive. Initially, we consider the case that when the robot is moving in the forward direction with $\dot{p}_x > 0$ and $\ddot{p}_x > 0$, which means that $\dot{x}_i > 0$ and $\ddot{x}_i > 0$, and therefore the products $F^a_x(\theta_i)\ddot{x}_i$ and $F^d_x(\theta_i)\dot{x}_i$ are always positive. Hence, we can conclude that in this case these products are not contributing to the forward propulsion of the robot. In addition, it is easily seen that when the robot is moving forward with $\dot{p}_x > 0$ and $\ddot{p}_x < 0$, which means that $\dot{x}_i > 0$ and $\ddot{x}_i < 0$, the product $F^a_x(\theta_i)\ddot{x}_i$ is contributing to the forward propulsion of the robot. Note that the magnitude of the propulsive force increases by decreasing the linear acceleration of the link in the forward direction, $\ddot{x}_i$.

Now, what remains is to analyse the effects of the products $F^a_{xy}(\theta_i)\ddot{y}_i$ and $F^d_{xy}(\theta_i)\dot{y}_i$. A plot of $F^a_{xy}(\theta_i)$ for different values of μ_n is shown in Fig. 1a, while a plot of $F^d_{xy}(\theta_i)$ for different values of c_n and $c_t = 1$ is shown in Fig. 1b. In each plot, the angle between the link and the forward direction, θ_i, is varied from -90^o to 90^o. We see that when $c_n = c_t$, i.e. the drag

coefficients are equal, there is no effect on the propulsive force of the underwater snake robot due to the drag effect, since this gives $F^d_{xy}(\theta_i) = 0$. It is easily seen (Fig. 1b) that when the $c_n > c_t$ the component $F^d_{xy}(\theta_i)$ is negative as long as θ_i is positive, and vice versa. This means that the product $F^d_{xy}(\theta_i)\dot{y}_i$ is negative as long as $\text{sgn}(\theta_i) = \text{sgn}(\dot{y}_i)$. In addition, from Fig. 1a it is seen that for any positive value of μ_n the component $F^a_{xy}(\theta_i)$ is negative as long as θ_i is positive, and vice versa. It should be noted that the only case that $F^a_{xy}(\theta_i) = 0$ is the case where the parameter $\mu_n = 0$, i.e. the case where the added mass effects are neglectable. Hence, we can conclude that for any positive values of parameters μ_n the product $F^a_{xy}(\theta_i)\dot{y}_i$ is negative as long as $\text{sgn}(\theta_i) = \text{sgn}(\ddot{y}_i)$.

Additionally, we see that for a given $\ddot{y}_i$ and $\dot{y}_i$, a link produces its highest propulsive force when it forms an angle of $\pm 45^{\text{o}}$ with the forward direction of motion. It should be noted that the magnitude of the propulsive force becomes greater by increasing c_n with respect to c_t, or by increasing the magnitude of the sideways link velocity, $\dot{y}_i$, by increasing the parameter μ_n, or by increasing the magnitude of the sideways link acceleration, $\ddot{y}_i$ and by increasing the parameter μ_n, or by decreasing the linear acceleration of the link in the forward direction, $\dot{x}_i$.

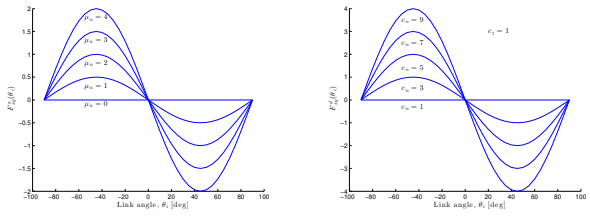

(a) Added mass component (b) Drag effect component

Fig. 1: The mapping from the sideways link motion to the forward propulsion for different fluid coefficients

Remark 1: In Fig. 1 we present the mapping from the sideways link motion to the forward propulsion for some fluid coefficients values without missing the generality of the analysis [2].

Now, we can summarize the properties of an underwater snake robot locomotion based on the previous analysis.

Property 1: For an underwater snake robot described by (3) with $c_n > c_t$, $\mu_n > 0$, $\dot{x}_i > 0$ and $\ddot{x}_i > 0$ forward propulsion is produced by link velocity and link acceleration components that are normal to the forward direction.

Property 2: For an underwater snake robot described by (3) with $c_n > c_t$, $\mu_n > 0$, $\dot{x}_i > 0$ and $\ddot{x}_i > 0$, the propulsive force generated by the transversal motion of link i is positive as long as $\text{sgn}(\theta_i) = \text{sgn}(\dot{y}_i)$ and $\text{sgn}(\theta_i) = \text{sgn}(\ddot{y}_i)$.

Property 3: For an underwater snake robot described by (3) with $c_n > c_t$, $\mu_n > 0$, $\dot{x}_i > 0$ and $\ddot{x}_i > 0$, the magnitude of the propulsive force produced by link i increases when $|\theta_i|$ increases as long as $|\theta_i| < 45^{\text{o}}$.

Property 4: For an underwater snake robot described by (3) with $c_n > c_t$, $\mu_n > 0$, $\dot{x}_i > 0$ and $\ddot{x}_i < 0$ forward propulsion is produced by link velocity and link acceleration components that are normal to the forward direction and also by the linear acceleration of the links in the forward direction.

It is worth mentioning that these results are general, because no assumptions have been made concerning the actual motion pattern of the underwater snake robot.

B. Analysis of turning locomotion

In the previous subsection, we determined how propulsion is generally achieved with an underwater snake robot, while in this subsection we will investigate how turning motion is achieved through simulations. In particular, we will investigate the turning motion for the two most common locomotion patterns for swimming snakes: In the first case the underwater snake robot moves by lateral undulation and in the second case the robot moves by eel-like undulation. Both gait patterns, lateral undulation and eel-like undulation, consist of horizontal waves that are propagated backward along the underwater snake body from head to tail, with the difference that in the latter the amplitude of the wave increases from the head to tail. The lateral undulation is realized by controlling each joint of the robot according to

$$\phi^*_i = \alpha \sin(\omega t + (i-1)\beta) + \phi_0, \quad i = 1, \ldots, n-1, \tag{5}$$

where the parameter α corresponds to the amplitude of the serpentine wave that propagates along the body of the snake robot, ω is the angular frequency of the sinusoidal joint motion, β determines the phase shift between the sequential joints, and ϕ_0 is the joint offset that is used to control the direction of the motion.

The eel-like motion is achieved by propagating lateral axial undulations with increasing amplitude from nose to tail. A simple equation is considered for the eel-like motion by controlling each joint of the snake robot according to the reference signal (see. e.g. [1])

$$\phi^*_i = \alpha \left(\frac{n-i}{n+1}\right) \sin(\omega t + (i-1)\beta) + \phi_0, \quad i = 1, \ldots, n-1, \tag{6}$$

where the parameter $\alpha(n-i)/(n+1)$ corresponds to the increasing amplitude, from nose to tail. In both cases, the parameter ϕ_0 is a joint angle offset value that controls the overall direction of the locomotion. The effect of changing this parameter is illustrated in Fig. 2 for lateral undulation and eel-like motion. This presents the results of a simulation of an underwater snake robot described by (3) with $N = 10$ links of length $l = 0.14$ m.

The trace of the head is shown in Fig. 2a-2b, while the average joint angle, defined as $\bar{\phi} = \sum_{i=1}^{N-1} \phi_i/(N-1)$, is shown in Fig. 2c-2d. The underwater snake robot is controlled according to lateral undulation, (5), and eel-like motion, (6), with $\alpha = 30^{\text{o}}$, $\omega = 120^{\text{o}}/\text{s}$ and $\beta = 40^{\text{o}}$. In addition, the offset angle is set to $\phi_0 = 5^{\text{o}}$ in the time interval $t \in [20, 30]$ and $\phi_0 = -10^{\text{o}}$ in the time interval $t \in [50, 60]$, while the offset angle is set to $\phi_0 = 0^{\text{o}}$ outside these two time intervals.

From Fig. 2, we can see that the robot swims forward without turning as long as the average joint angle, $\bar{\phi}$, is oscillates around zero, while the direction of the motion changes when the average joint angle is non-zero. It is seen (Fig. 2) that in the case of eel-like motion the average joint angle oscillates with larger amplitude compared to lateral undulation around the expected direction. The positive (resp. negative) average joint angle produces a counterclockwise (resp. clockwise) rotation of the underwater snake robot.

In addition, we can see that the speed of the directional change is correlated with the amplitude of the average joint angle. Moreover, Fig. 2a-2b show that the rate of directional change is larger when the robot moves with larger forward velocity (for $\omega = 120^{o}/\text{s}$). This indicates that the speed of the directional change, for some fixed joint angle offset, becomes greater by increasing the forward velocity of the underwater snake robot. Through the simulation study based on the complex model we observe a set of qualitative properties and similar formulations as the ones that observed for the ground snake robot locomotion presented in [2], [14]. We will now summarize the observations of this simulation study of the turning locomotion of an underwater snake robot.

Proposition 1: During both lateral undulation and eel-like motion for an underwater snake robot described by (3) with $c_n > c_t$ and $\mu_n > 0$, the overall direction of the locomotion remains constant as long as the average joint angle is zero. However, this will change in the counterclockwise (resp. clockwise) direction when the average joint angle is positive (resp. negative). The speed of directional change of the locomotion becomes greater by increasing the amplitude of the average joint angle and/or by increasing the forward velocity (assuming that the average joint angle is non-zero).

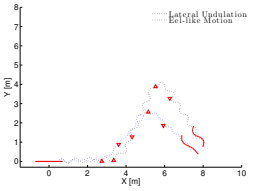

(a) Trace of the head for $\omega = 70^{o}/\text{s}$

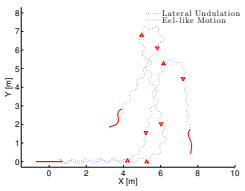

(b) Trace of the head for $\omega = 120^{o}/\text{s}$

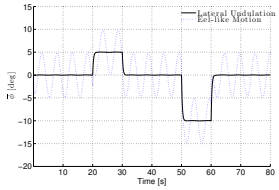

(c) The averaged ϕ for $\omega = 70^{o}/\text{s}$

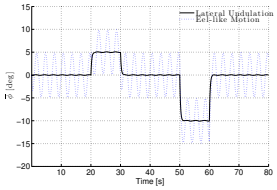

(d) The averaged ϕ for $\omega = 120^{o}/\text{s}$

Fig. 2: Turning Locomotion Analysis

C. Analysis of link motion

From the analysis in Section III.A it is clear that underwater snake locomotion consists of periodic body shape changes that generate external forces that propel the robot forward. According to the Property 1, the forward motion is inducted by the motion of the links normal to the forward direction. The above result led us to wonder if the body shape changes can be characterized in terms of the translational displacements of the links instead of the rotational joints motion. This would be similar to the approach presented for the ground snake robot in [2], [14]. Generally, the model given by (3), which describes the rotational link motion of an underwater snake robot, is quite complex.

In order to support this idea, we consider an underwater snake robot described by (3) forced to move with lateral undulation, (5), and eel-like motion, (6), along the global x axis with $\phi_0 = 0^{o}$. Fig. 3 show the relative displacement between the CM of two arbitrarily chosen links (link 3 and link 4) in the global x and y directions. These plots indicate that, during both lateral undulation and eel-like motion, the relative displacements between the CM of two adjacent links along the forward direction of motion are approximately constant, while the relative displacements normal to the direction of motion oscillate around zero. Hence, based on these simulation results we can compose the following proposition.

Proposition 2: During both lateral undulation and eel-like motion, the change in body shape consists mainly of relative displacement of the CM of the links normal to the direction of motion. In addition, the relative displacement of the CM of the links along the forward direction can be approximated as constant.

Remark 2: The analysis of the underwater snake robot locomotion gives Property 1-4 and Proposition 1-2, which are similar to the ones presented in [2], [14] for a ground snake robot. However, in this paper, the properties are developed under the assumption that the snake robot moves according to lateral undulation and eel-like motion, and also the hydrodynamic effects are analyzed.

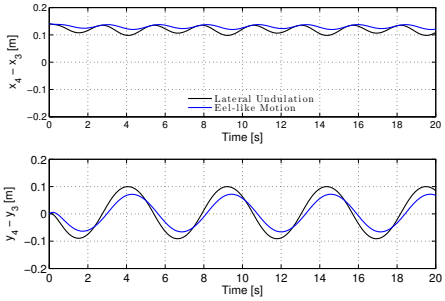

Fig. 3: Relative displacement of the CM of link 3 and 4

IV. A CONTROL–ORIENTED MODEL OF AN UNDERWATER SNAKE ROBOT

Using the results from the previous section, we now develop a control-oriented model of an underwater snake robot moving in a virtual horizontal plane. The model is derived for control design and stability analysis purposes.

A. Overview of the modeling approach

The idea behind the control-oriented model of underwater snake robot locomotion is based on the simplified modeling approach presented in [2], [14] for a ground snake robot. In particular the idea is to describe the body shape changes of an underwater snake robot as linear displacements of the links with respect to each other instead of rotational displacements. Proposition 2 indicates that these linear displacements should be normal to the forward direction of the motion, while Property 1 points out that these transversal displacements of the links are that which propel the underwater snake robot forward. This suggest that we can model the revolute joints of an underwater snake robot as prismatic (translational) joints.

In the following subsections, the kinematics and dynamics of the underwater snake robot will be modeled in terms of the mathematical symbols described in Table I and illustrated in Fig. 4a-4b. The following vectors and matrices are used in order to derive the model.

TABLE I: Definition of mathematical terms

Symbol	Description
N	The number of links
l	The length of a link
m	Mass of each link
ϕ_i	Normal direction distance between links i and $i+1$
$\upsilon_{\phi,i}$	Relative velocity between links i and $i+1$
θ	Orientation of the underwater snake robot
υ_θ	Angular velocity of the underwater snake robot
(t_i, n_i)	Coordinates of the CM of link i in the $t-n$ frame
(p_t, p_n)	Coordinates of the CM of the robot in the $t-n$ frame
(p_x, p_y)	Coordinates of the CM of the robot in the global frame
(υ_t, υ_n)	Forward and normal direction velocity of the robot
u_i	Actuator force at joint i
$(f_{x,i}, f_{y,i})$	Fluid force on link i in the global frame
$(f_{t,i}, f_{n,i})$	Fluid force on link i in the $t-n$ frame

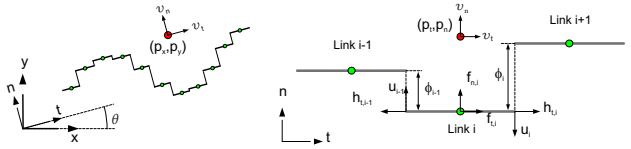

(a) The control-oriented model (b) Kinematics and dynamics of the robot

Fig. 4: Underwater snake robot

$$\mathbf{A} = \begin{bmatrix} 1 & 1 & & \\ & \ddots & \ddots & \\ & & 1 & 1 \end{bmatrix}, \mathbf{D} = \begin{bmatrix} 1 & -1 & & \\ & \ddots & \ddots & \\ & & 1 & -1 \end{bmatrix},$$

$$\mathbf{e} = \begin{bmatrix} 1 & \dots & 1 \end{bmatrix}^T \in \mathbb{R}^N, \bar{\mathbf{e}} = \begin{bmatrix} 1 & \dots & 1 \end{bmatrix}^T \in \mathbb{R}^{N-1},$$

$$\bar{\mathbf{D}} = \mathbf{D}^T \left(\mathbf{D}\mathbf{D}^T\right)^{-1} \in \mathbb{R}^{N\times N-1},$$

where $\mathbf{A}, \mathbf{D} \in \mathbb{R}^{(N-1)\times N}$.

B. Kinematics of the underwater snake robot

The underwater snake robot is assumed to move in a horizontal plane, fully immersed in water, and has N+2 degrees of freedom. The motion of the robot is defined with respect to the fixed global frame, $x-y$, and the $t-n$ frame that is always aligned with the robot (Fig. 4a) The origin of both frames are fixed and coincide. The direction of the t axis is denoted as the tangential or forward direction of the robot, and the direction of the n axis as the normal direction. As shown in Fig. 4, the global frame position of the CM of the underwater snake robot is denoted by $(p_x, p_y) \in \mathbb{R}^2$, while $(p_t, p_n) \in \mathbb{R}^2$ is the $t-n$ frame position. $\theta \in \mathbb{R}$ stands for the global frame orientation and is expressed with respect to the global x axis with counterclockwise positive direction. The angle between the global x axis and the t axis is also θ since the $t-n$ frame is always aligned with the snake robot. The relationship between the $t-n$ frame position and the global frame position is given by

$$p_t = p_x \cos\theta + p_y \sin\theta, \quad p_n = -p_x \sin\theta + p_y \cos\theta \tag{7}$$

The relationship between the global frame velocity of the robot and the $t-n$ frame velocities is given by

$$\dot{p}_x = \upsilon_t \cos\theta - \upsilon_n \sin\theta, \quad \dot{p}_y = \upsilon_t \sin\theta + \upsilon_n \cos\theta, \tag{8}$$

and the inverse relationship is given by

$$\upsilon_t = \dot{p}_x \cos\theta + \dot{p}_y \sin\theta, \quad \upsilon_n = -\dot{p}_x \sin\theta + \dot{p}_y \cos\theta. \tag{9}$$

Differentiating (7) with respect to time and inserting (9) gives

$$\dot{p}_t = \upsilon_t + p_n\dot{\theta}, \quad \dot{p}_n = \upsilon_n - p_t\dot{\theta}. \tag{10}$$

We denote the $t-n$ frame position of the CM of the link i by $(t_i, n_i) \in \mathbb{R}^2$. The $N-1$ prismatic joints of the underwater snake robot control the normal direction distance between the links. As sees in the Fig. 4b, the normal direction distance between the link i and link $i+1$ is given by

$$\phi_i = n_{i+1} - n_i \tag{11}$$

and represents the coordinate of joint i. In the control-oriented, we refer to ϕ_i as a joint coordinate instead of a joint angle. The holonomic constraints is expressed in matrix form for all links as

$$\mathbf{D}\mathbf{t} + l\bar{\mathbf{e}} = \mathbf{0}, \quad \mathbf{D}\mathbf{n} + \phi = \mathbf{0}, \tag{12}$$

where $\mathbf{t} = [t_1, \dots, t_N] \in \mathbb{R}^N$, $\mathbf{n} = [n_1, \dots, n_N] \in \mathbb{R}^N$, and $\phi = [\phi_1, \dots, \phi_{N-1}] \in \mathbb{R}^{N-1}$. The $t-n$ frame position of the CM of the underwater snake robot can be written in terms of the link positions as

$$p_t = \mathbf{e}^T\mathbf{t}/N, \quad p_n = \mathbf{e}^T\mathbf{n}/N, \tag{13}$$

The link positions can be expressed as

$$\mathbf{t} = p_t\mathbf{e} - l\bar{\mathbf{D}}\bar{\mathbf{e}}, \quad \mathbf{n} = p_n\mathbf{e} - \bar{\mathbf{D}}\phi. \tag{14}$$

By differentiating (14) with respect to time and inserting (10), the individual link velocities are given as

$$\dot{\mathbf{t}} = (\upsilon_t + p_n\dot{\theta})\mathbf{e}, \quad \dot{\mathbf{n}} = (\upsilon_n - p_t\dot{\theta})\mathbf{e} - \bar{\mathbf{D}}\dot{\phi}. \tag{15}$$

The kinematics of an underwater snake robot, described in this subsection, is similar to that of a snake robot moving on land. In this section we provide a brief presentation of the kinematics for completeness. An extensive presentation of the snake robot kinematics can be found in [2], [14]. Additionally, it is necessary to derive the equations of linear accelerations of the links in order to express the fluid forces below. Hence, the linear accelerations of the links are found by differentiating the velocity of the individual links (15) with respect to time, which gives

$$\ddot{\mathbf{t}} = (\dot{\upsilon}_t + \dot{p}_n\dot{\theta} + p_n\ddot{\theta})\mathbf{e}, \quad \ddot{\mathbf{n}} = (\dot{\upsilon}_n - \dot{p}_t\dot{\theta} - p_t\ddot{\theta})\mathbf{e} - \bar{\mathbf{D}}\ddot{\phi}. \tag{16}$$

C. Fluid dynamic model

In this subsection, we employ a fluid model that takes into account the added mass effects and linear drag forces, similar to the hydrodynamic model described in Section II. The hydrodynamic forces, which act on the CM of each link, must be defined so that Property 1-3 from Section III be also applicable for the control-oriented model of the robot.

By assembling the forces in (1) on all links in vector form, we can rewrite the global frame fluid forces on the links as

$$\mathbf{f} = \begin{bmatrix} \mathbf{f_x} \\ \mathbf{f_y} \end{bmatrix} = \begin{bmatrix} \mathbf{f_{A_x}} \\ \mathbf{f_{A_y}} \end{bmatrix} + \begin{bmatrix} \mathbf{f_{D_x}} \\ \mathbf{f_{D_y}} \end{bmatrix}, \tag{17}$$

where $\mathbf{f_{A_x}}$ and $\mathbf{f_{A_y}}$ represent the effects from added mass forces and are expressed as

$$\begin{bmatrix} \mathbf{f_{A_x}} \\ \mathbf{f_{A_y}} \end{bmatrix} = -\begin{bmatrix} \mu_n(\mathbf{S}_\theta)^2 & -\mu_n\mathbf{S}_\theta\mathbf{C}_\theta \\ -\mu_n\mathbf{S}_\theta\mathbf{C}_\theta & \mu_n(\mathbf{C}_\theta)^2 \end{bmatrix} \begin{bmatrix} \ddot{\mathbf{X}} \\ \ddot{\mathbf{Y}} \end{bmatrix}, \tag{18}$$

where $\mathbf{S}_\theta = \mathrm{diag}(\sin\theta)$ and $\mathbf{C}_\theta = \mathrm{diag}(\cos\theta)$ The vectors $\mathbf{f_{D_x}}$, $\mathbf{f_{D_y}}$ present the effects from the linear drag forces (19).

$$\begin{bmatrix} \mathbf{f_{D_x}} \\ \mathbf{f_{D_y}} \end{bmatrix} = -\begin{bmatrix} c_t(\mathbf{C}_\theta)^2 + c_n(\mathbf{S}_\theta)^2 & (c_t - c_n)\mathbf{S}_\theta\mathbf{C}_\theta \\ (c_t - c_n)\mathbf{S}_\theta\mathbf{C}_\theta & c_t(\mathbf{S}_\theta)^2 + c_n(\mathbf{C}_\theta)^2 \end{bmatrix} \begin{bmatrix} \dot{\mathbf{X}} \\ \dot{\mathbf{Y}} \end{bmatrix} \tag{19}$$

Assumption 1: When θ_i is small, the following approximations hold $\sin^2\theta_i \approx 0$, $\cos^2\theta_i \approx 1$ and $\sin\theta_i\cos\theta_i \approx \theta_i$ (see e.g. [14]).

Remark 3: Assumption 1 is valid for $(|\,\theta_i\,| < 20^o)$ as it is shown in [2], [14]. We will therefore approximate the added mass and drag forces based on this assumption.

The velocities $\dot{x}_i$ and $\dot{y}_i$ correspond to the velocity of link i in the tangential and normal directions of the underwater

snake robot, respectively, the forces $f_{x,i}$ and $f_{y,i}$ correspond to the fluid forces on link i in the tangential and normal directions, respectively. By denoting the fluid force components on link i in the $t-n$ frame of the control-oriented model by $f_{t,i}$ and $f_{n,i}$, respectively and letting the $t-n$ frame velocity and acceleration components of link i be given by $(\dot{t}_i,\ \dot{n}_i)$ and $(\ddot{t}_i,\ \ddot{n}_i)$, we then have that

$$\dot{x}_i = \dot{t}_i,\ \dot{y}_i = \dot{n}_i,\ \ddot{x}_i = \ddot{t}_i,\ \ddot{y}_i = \ddot{n}_i,\ f_{x,i} = f_{t,i},\ f_{y,i} = f_{n,i}. \tag{20}$$

Using Ass. 1 and $\theta_i \approx (\phi_{i-1}+\phi_i)/2l$ (see e.g. [2], [14]), the fluid forces in the tangential, $\mathbf{f_t} \in \mathbb{R}^N$, and normal, $\mathbf{f_n} \in \mathbb{R}^N$, directions can be written as

$$\begin{bmatrix} \mathbf{f_t} \\ \mathbf{f_n} \end{bmatrix} = \begin{bmatrix} \mathbf{f_{A_t}} \\ \mathbf{f_{A_n}} \end{bmatrix} + \begin{bmatrix} \mathbf{f_{D_t}} \\ \mathbf{f_{D_n}} \end{bmatrix}, \tag{21}$$

where

$$\begin{bmatrix} \mathbf{f_{A_t}} \\ \mathbf{f_{A_n}} \end{bmatrix} = - \begin{bmatrix} \mathbf{0}_{N\times N} & -\frac{\mu_n}{2l}\mathrm{diag}(\mathbf{A}^T\phi) \\ -\frac{\mu_n}{2l}\mathrm{diag}(\mathbf{A}^T\phi) & \mu_n \mathbf{I}_N \end{bmatrix} \begin{bmatrix} \ddot{\mathbf{t}} \\ \ddot{\mathbf{n}} \end{bmatrix}_{\dot{\theta}=0,\ddot{\theta}=0} \tag{22}$$

and

$$\begin{bmatrix} \mathbf{f_{D_t}} \\ \mathbf{f_{D_n}} \end{bmatrix} = \begin{bmatrix} -c_t \mathbf{I}_N & c_p\mathrm{diag}(\mathbf{A}^T\phi) \\ c_p\mathrm{diag}(\mathbf{A}^T\phi) & -c_n\mathbf{I}_N \end{bmatrix} \begin{bmatrix} \dot{\mathbf{t}} \\ \dot{\mathbf{n}} \end{bmatrix}_{\dot{\theta}=0}. \tag{23}$$

The parameter $c_p = (c_n - c_t)/2l$ is a propulsion coefficient which maps the normal direction link velocities and the joint coordinates into propulsive fluid forces in the forward (tangential) direction of the underwater snake robot.

Remark 4: We can seen from (22) and (23) that the propulsive force on link i that propel the robot forward are produced by the normal direction link velocity, $\dot{n}_i$, and by the normal direction link acceleration, $\ddot{n}_i$, which is in agreement with Property 1. Furthermore, we see from (22) and (23) that the magnitude of the propulsive forces produced by link i is increased by increasing $\mid \phi_{i-1}+\phi_i \mid$, which from $\theta_i \approx (\phi_{i-1}+\phi_i)/2l$, corresponds to increasing $\mid \theta_i \mid$. This is in agreement with Property 3. Finally, we can see from (22) and (23) that the forward direction force components produced by $\dot{n}_i$ and $\ddot{n}_i$ is positive when $\mathrm{sgn}(\phi_{i-1}+\phi_i) = \mathrm{sgn}(\dot{n}_i)$ and $\mathrm{sgn}(\phi_{i-1}+\phi_i) = \mathrm{sgn}(\ddot{n}_i)$, which is in agreement with Property 2. Hence, we conclude that the simplified/control-oriented fluid model directly captures the Property 1-3 from Section III.A, which means that we can argue that the simplified fluid model in (22), (23) is qualitatively similar to the complex fluid model in (17).

Remark 5: In this control-oriented modeling approach we choose to disregard the link velocity components due to the angular velocity $\dot{\theta}$ of the underwater snake robot and the link acceleration components $\ddot{\theta}$, due to the angular velocity. These are reasonable assumptions since the dynamics of the angular motion of the underwater snake robot will generally be much slower than the body shape dynamics. Furthermore, these assumptions simplify the fluid model significantly.

Inserting (15) into (22) and (16) into (23) with $\dot{\theta} = 0$ and $\ddot{\theta} = 0$ the final expressions for the added mass effects and linear drag forces can be written as

$$\begin{aligned} \begin{bmatrix} \mathbf{f_{A_t}} \\ \mathbf{f_{A_n}} \end{bmatrix} = &- \begin{bmatrix} \mathbf{0}_{N\times N} & -\frac{\mu_n}{2l}\mathrm{diag}(\mathbf{A}^T\phi)\mathbf{e} \\ -\frac{\mu_n}{2l}\mathrm{diag}(\mathbf{A}^T\phi)\mathbf{e} & \mu_n\mathbf{I}_N\mathbf{e} \end{bmatrix} \begin{bmatrix} \dot{\upsilon}_t \\ \dot{\upsilon}_n \end{bmatrix} \\ &- \begin{bmatrix} \mathbf{0}_{N\times N} & -\frac{\mu_n}{2l}\mathrm{diag}(\mathbf{A}^T\phi) \\ -\frac{\mu_n}{2l}\mathrm{diag}(\mathbf{A}^T\phi) & \mu_n\mathbf{I}_N \end{bmatrix} \begin{bmatrix} \mathbf{0}_N \\ -\bar{\mathbf{D}}\ddot{\phi} \end{bmatrix} \end{aligned} \tag{24}$$

and

$$\begin{bmatrix} \mathbf{f_{D_t}} \\ \mathbf{f_{D_n}} \end{bmatrix} = \begin{bmatrix} -c_t\upsilon_t\mathbf{e} + c_p\mathrm{diag}(\mathbf{A}^T\phi)(\upsilon_n\mathbf{e} - \bar{\mathbf{D}}\dot{\phi}) \\ -c_n\upsilon_n\mathbf{e} + c_n\bar{\mathbf{D}}\dot{\phi} + c_p\upsilon_t\mathrm{diag}(\mathbf{A}^T\phi)\mathbf{e} \end{bmatrix}. \tag{25}$$

D. Dynamics of the underwater snake robot

This subsection presents the equations of motion for the underwater snake robot. The forces and torques acting on link i are visualized in Fig. 4b and the force balance for link i in global frame coordinates is given by

$$m\ddot{t}_i = f_{t,i} + h_{t,i} - h_{t,i-1}, \quad m\ddot{n}_i = f_{n,i} - u_i + u_{i-1} \tag{26}$$

where $f_{t,i}$ and $f_{n,i}$ are the fluid forces, $h_{t,i}$ and $h_{t,i-1}$ are the joint constraint forces on link i from link $i+1$ and link $i-1$, respectively, and u_i and u_{i-1}, produce relative motion between the links in the normal direction. The force balance equations for all links may be expressed in matrix form as

$$m\ddot{\mathbf{t}} = \mathbf{f_t} + \mathbf{D}^T\mathbf{h}_t, \tag{27}$$

$$m\ddot{\mathbf{n}} = \mathbf{f_n} - \mathbf{D}^T\mathbf{u}, \tag{28}$$

where $\mathbf{h}_t = [h_{t,1},\ldots,h_{t,N-1}]^T \in \mathbb{R}^{N-1}$ and $\mathbf{u} = [u_1,\ldots,u_{N-1}]^T \in \mathbb{R}^{N-1}$. Premultiplying (28) by $\mathbf{D}/m$ gives

$$\mathbf{D}\ddot{\mathbf{n}} = \frac{1}{m}\mathbf{D}\mathbf{f_n} - \frac{1}{m}\mathbf{D}\mathbf{D}^T\mathbf{u}. \tag{29}$$

By differentiating (12) twice with respect to time, it is seen that $\mathbf{D}\ddot{\mathbf{n}} = -\ddot{\phi}$. We can therefore write the body shape dynamics of the underwater snake robot as

$$\ddot{\phi} = -\frac{1}{m}\mathbf{D}\mathbf{f_n} + \frac{1}{m}\mathbf{D}\mathbf{D}^T\mathbf{u}. \tag{30}$$

Inserting (21) into (30) and using the easily verifiable relations $\mathbf{D}\mathbf{e} = 0$, $\mathbf{D}\bar{\mathbf{D}} = \mathbf{I}_{N-1}$, $\mathbf{D}\mathrm{diag}(\mathbf{A}^T\phi)\mathbf{e} = -\mathbf{A}\mathbf{D}^T\phi$, we get

$$\ddot{\phi} = -\frac{c_n}{m+\mu_n}\dot{\phi} + \frac{1}{m+\mu_n}\left(\frac{\mu_n}{2l}\mathbf{A}\mathbf{D}^T\dot{\upsilon}_t + c_p\mathbf{A}\mathbf{D}^T\upsilon_t\right)\phi + \frac{1}{m+\mu_n}\mathbf{D}\mathbf{D}^T\mathbf{u}. \tag{31}$$

The tangential and normal direction accelerations of the CM of the underwater snake robot, denoted by $\dot{\upsilon}_t$ and $\dot{\upsilon}_n$, respectively, are given as the sum of all tangential and normal direction forces on the links divided by its mass. This gives

$$\begin{bmatrix} \dot{\upsilon}_t \\ \dot{\upsilon}_n \end{bmatrix} = \frac{1}{Nm}\begin{bmatrix} \mathbf{e}^T & \mathbf{0}_{N\times N} \\ \mathbf{0}_{N\times N} & \mathbf{e}^T \end{bmatrix}\begin{bmatrix} \mathbf{f_t} \\ \mathbf{f_n} \end{bmatrix}, \tag{32}$$

where we can see that the joint constraint forces, $\mathbf{h}_t$, and the actuator forces, $\mathbf{u}$, are cancelled out when the link accelerations are summed. Now, inserting (21) into (32) and using easily verifiable relations, $\mathbf{e}^T\mathrm{diag}(\mathbf{A}^T\phi)\mathbf{e} = 2\bar{\mathbf{e}}^T\phi$, $\mathbf{e}^T\bar{\mathbf{D}} = 0$, and $\mathbf{e}^T\mathrm{diag}(\mathbf{A}^T\phi)\bar{\mathbf{D}} = \phi^T\mathbf{A}\bar{\mathbf{D}}$, we get

$$\begin{aligned} \dot{\upsilon}_t &= k_3\left(k_1 2c_p(\bar{\mathbf{e}}^T\phi)^2 - k_2c_tN\right)\upsilon_t + k_3\left(k_2 2c_p\bar{\mathbf{e}}^T\phi - k_1c_nN\bar{\mathbf{e}}^T\phi\right)\upsilon_n \\ &\quad - k_3(k_2\frac{k_1}{2}\phi^T\mathbf{A}\bar{\mathbf{D}}\ddot{\phi} + k_2c_p\phi^T\mathbf{A}\bar{\mathbf{D}}\dot{\phi}) \\ \dot{\upsilon}_n &= k_3\left(Nm2c_p\bar{\mathbf{e}}^T\phi - k_1c_tN\bar{\mathbf{e}}^T\phi\right)\upsilon_t + k_3\left(k_1 2c_p(\bar{\mathbf{e}}^T\phi)^2 - N^2mc_n\right)\upsilon_n \\ &\quad - \bar{\mathbf{e}}^T\phi k_3(k_1c_p\phi^T\mathbf{A}\bar{\mathbf{D}}\dot{\phi} + \frac{{k_1}^2}{2}\phi^T\mathbf{A}\bar{\mathbf{D}}\ddot{\phi}) \end{aligned} \tag{33}$$

where $k_1 = \mu_n/l$, $k_2 = Nm + N\mu_n$ and $k_3 = \dfrac{1}{Nmk_2 - (k_1\bar{\mathbf{e}}^T\phi)^2}$. (34)

We also need to model the dynamics of the snake robot orientation. As mentioned in previous sections, the idea behind the control-oriented modeling approach of the underwater snake robot locomotion is to disregard the rotational motion of the links and instead only consider the translational displacements of the links. The orientation of the robot with prismatic joints is defined as θ, which is also the angle of all the links.

Proposition 1 states that the direction of the forward motion changes when the average of the joint angles is

oscillates around a non-zero value and that the speed of direction changes is increased by increasing the average of the joint angles and/or by increasing the forward velocity. This observation should also hold for the control-oriented model. The direction of the forward motion in the control-oriented model is given by the orientation θ, the forward velocity is given by υ_t, and the average of the joint angles corresponds to the average of the joint coordinates $\bar{\mathbf{e}}^T\phi/(N-1)$. Hence, using Prop. 1, the overall torque that induces the rotational motion of a snake robot should be

$$\ddot{\theta}_{rotation} = \lambda_2 \upsilon_t \frac{\bar{\mathbf{e}}^T\phi}{N-1} \tag{35}$$

where λ_2 is a constant parameter which gives the scaling of the mapping from average coordinate and forward velocity to rotational acceleration. The induced torque is multiplied by υ_t since the snake robot otherwise would experience a constant angular velocity, even in the case of a nonzero average joint coordinate in the rest mode. Furthermore, fluid forces act on the underwater snake robot in order to induce fluid torques that oppose the rotational motion. Since the fluid forces are the linear drag forces and added mass effects, we can assume that the rotational fluid torques are obtained due to the added mass and the linear drag forces. We choose to model the torque due to the added mass effect as

$$\ddot{\theta}_{am} = -\lambda_3 \ddot{\theta}, \tag{36}$$

where λ_3 is a constant parameter which indicates the torque coefficient due to the added mass effect. In addition, we model the torque due to the linear drag forces as

$$\ddot{\theta}_{drag} = -\lambda_1 \dot{\theta}, \tag{37}$$

where λ_1 is a constant parameter which determines the drag torque opposing to the rotation of the underwater snake robot. By combining (35), (36) and (37) we can write the control-oriented model of the rotational dynamics of the underwater snake robot as

$$\ddot{\theta} = -\frac{\lambda_1}{1+\lambda_3}\dot{\theta} + \frac{\lambda_2}{(N-1)(1+\lambda_3)}\upsilon_t \bar{\mathbf{e}}^T\phi, \tag{38}$$

Remark 6: Although, the model of $\ddot{\theta}$ is not based on first principles of the rotational dynamics (see e.g. [2]) of an underwater snake robot, we can presume that the behavior of this model will be qualitatively similar to the behavior of an underwater snake robot with revolute joints. It will also be quantitatively similar when the rotation parameters λ_1, λ_2 and λ_3 are properly chosen. This claim will be supported by simulation results in the following section.

E. Complete control-oriented model

We now present the complete control-oriented model of the underwater snake robot. The state vector of the model is chosen as

$$\mathbf{x} = \left[\phi^T, \theta, p_x, p_y, \mathbf{v}_\phi^T, \upsilon_\theta, \upsilon_t, \upsilon_n\right]^T \in \mathbb{R}^{2N+4}, \tag{39}$$

where $\phi \in \mathbb{R}^{N-1}$ are the joint coordinates, $\theta \in \mathbb{R}$ is the absolute orientation, $(p_x, p_y) \in \mathbb{R}^2$ is position of CM in the the global frame, $\mathbf{v}_\phi = \dot{\phi} \in \mathbb{R}^{N-1}$ are the joint velocities, $\upsilon_\theta = \dot{\theta} \in \mathbb{R}$ is the angular velocity, and $(\upsilon_t, \upsilon_n) \in \mathbb{R}^2$ are the tangential and normal direction velocities of the robot. As illustrated in Fig. 4b, each link is influenced by fluid forces, linear drag forces and the added mass effects, and constraint forces that hold the joints together. The complete control-oriented model of the robot can be written as

$$\dot{\phi} = \mathbf{v}_\phi \tag{40a}$$

$$\dot{\theta} = \upsilon_\theta \tag{40b}$$

$$\dot{p}_x = \upsilon_t \cos\theta - \upsilon_n \sin\theta \tag{40c}$$

$$\dot{p}_y = \upsilon_t \sin\theta + \upsilon_n \cos\theta \tag{40d}$$

$$\dot{\mathbf{v}}_\phi = -\frac{c_n N}{k_2}\mathbf{v}_\phi + \frac{N}{k_2}\left(\frac{k_1}{2}\mathbf{A}\mathbf{D}^T\dot{\upsilon}_t + c_p\mathbf{A}\mathbf{D}^T\upsilon_t\right)\phi + \frac{N}{k_2}\mathbf{D}\mathbf{D}^T\mathbf{u} \tag{40e}$$

$$\dot{\upsilon}_\theta = -\frac{\lambda_1}{1+\lambda_3}\upsilon_\theta + \frac{\lambda_2}{(N-1)(1+\lambda_3)}\upsilon_t\bar{\mathbf{e}}^T\phi \tag{40f}$$

$$\begin{aligned}\dot{\upsilon}_t = {} & k_3\left(k_1 2c_p(\bar{\mathbf{e}}^T\phi)^2 - k_2 c_t N\right)\upsilon_t + k_3\left(k_2 2c_p\bar{\mathbf{e}}^T\phi - k_1 c_n N\bar{\mathbf{e}}^T\phi\right)\upsilon_n \\ & - k_3\left(k_2\frac{k_1}{2}\phi^T\mathbf{A}\bar{\mathbf{D}}\dot{\mathbf{v}}_\phi + k_2 c_p\phi^T\mathbf{A}\bar{\mathbf{D}}\mathbf{v}_\phi\right)\end{aligned} \tag{40g}$$

$$\begin{aligned}\dot{\upsilon}_n = {} & k_3\left(Nm2c_p\bar{\mathbf{e}}^T\phi - k_1 c_t N\bar{\mathbf{e}}^T\phi\right)\upsilon_t + k_3\left(k_1 2c_p(\bar{\mathbf{e}}^T\phi)^2 - N^2 m c_n\right)\upsilon_n \\ & - \bar{\mathbf{e}}^T\phi k_3\left(k_1 c_p\phi^T\mathbf{A}\bar{\mathbf{D}}\mathbf{v}_\phi + \frac{{k_1}^2}{2}\phi^T\mathbf{A}\bar{\mathbf{D}}\dot{\mathbf{v}}_\phi\right)\end{aligned} \tag{40h}$$

where $\mathbf{u} \in \mathbb{R}^{N-1}$ are the transformed actuator forces at the joints.

Remark 7: It should be noted that in this paper the control-oriented model is derived based on Property 1-3 and the Proposition 1-2. This modeling approach is not able to capture the results in the case pointed in Property 4.

V. COMPARISON BETWEEN THE COMPLEX AND THE CONTROL–ORIENTED MODEL

This section presents simulation results for lateral undulation and eel-like motion in order to compare the complex underwater snake robot model given by (3) and the control-oriented model given by (40). Both models were implemented and simulated in Matlab R2011b. The dynamics was calculated using ode45 solver in Matlab with a relative and absolute error tolerance of 10^{-6}.

A. Simulation parameters

We consider an underwater snake robot has $N = 10$ links of length $l = 0.14$ m. The mass of each link is $m = 0.6597$ kg and it chosen to fulfil the neutrally buoyant assumption (cf. [1]). Furthermore, we choose the fluid forces and torque coefficients as $c_t = 0.2639$, $c_n = 4.2$, $\mu_n = 0.3957$, $\lambda_1 = 2.2988 \times 10^{-7}$, $\lambda_2 = 4.3103 \times 10^{-4}$, for the complex model and $c_t = 0.45$, $c_n = 5$, $\mu_n = 0.4$, $\lambda_1 = 0.5$, $\lambda_2 = 20$, $\lambda_3 = 0.01$ for the control-oriented. Please note that defining a general mapping between the fluid coefficients in the two models remains a topic of future work. The coefficients here are chosen through trial and error. The joint reference coordinates were calculated according to the motion pattern lateral undulation and eel-like motion, defined in (5) and (6), respectively. The values of the controller parameters are set $\omega = 120^o/\text{s}$, $\beta = 40^o$ in both models, while the values of parameter α are presented with each simulation results. In addition, the joint offset angle was set to $\phi_0 = \alpha/6$ in the time interval $t \in [40, 70]$, $\phi_0 = -\alpha/6$ in the time interval $t \in [130, 160]$ and $\phi_0 = 0$ outside of these two time intervals. Both models are simulated with the initial values set to zero. Furthermore, in order to achieve the desired locomotion patterns given in (5) and (6) we use the following PD-controller for both complex and control-oriented model:

$$\mathbf{u} = \ddot{\phi}^* + k_d(\dot{\phi}^* - \dot{\phi}) + k_p(\phi^* - \phi), \tag{41}$$

with the controller gains $k_p = 200$ and $k_d = 50$.

B. Simulation results

Simulation results for lateral undulation and eel-like motion of the underwater snake robot are presented. In particular, the amplitude of (5) and (6) is set to the values 13.9°, for the complex model and 4.3 cm for the control-oriented model. These amplitudes correspond to the link angle $\theta_i = 20^{\circ}$ (cf. [2] for details about how to transform between angular and translational link motion). The simulation results are shown in Fig. 5 for lateral undulation, while simulation results for eel-like motion are shown in Fig. 6. In all figures, the motion of CM for both models is presented in subfigure (a), while subfigures (b) and (c) show the CM velocity of the underwater snake robots in the global x and y direction, respectively. Furthermore, subfigure (d) shows the orientation of the underwater snake robots, which is given by θ in the control-oriented model, and is estimated as the average of the link angles in the complex model, i.e. as $\bar{\theta} = (1/N)\sum_{i=1}^{N} \theta_i$.

The simulation results, for both lateral undulation and eel-like motion, indicate that the qualitative behavior of the underwater robot expected by the control-oriented model is similar to the behavior corresponding to the complex model. In addition, choosing the presented values for the fluid coefficients, we also achieved a good quantitative similarity between the two models. The similar behavior of the two models confirms that the control-oriented model can capture all the effects that determine the overall motion of the underwater snake robot. Hence, the proposed control-oriented modeling approach could be used to develop a general analysis and control design, in order to get results that would be applicable for the complex model.

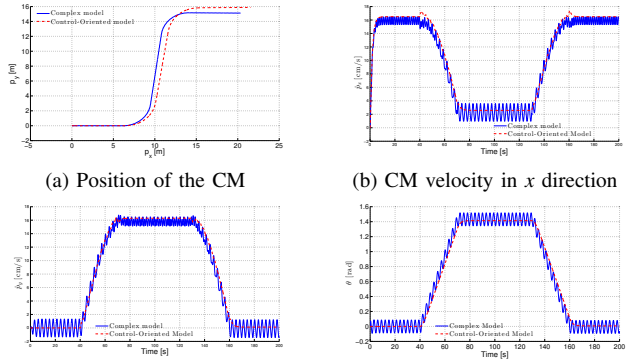

(a) Position of the CM (b) CM velocity in x direction

(c) CM velocity in y direction (d) The orientation

Fig. 5: Simulation results for lateral undulation

VI. CONCLUSIONS AND FUTURE WORK

This paper has presented a model of the kinematics and dynamics of a planar, underwater snake robot, aimed at control design and stability analysis purposes. The model, which takes into account the added mass effects, the linear drag forces, the torques due to the added mass and linear drag forces, is significantly less complex than the existing models on underwater snake robots. An extensive analysis of the complex model has been presented and a set of essential properties that characterize the overall motion of an underwater snake robot was derived. Simulation results for lateral undulation and eel-like motion indicate that the proposed control-oriented model captures these essential properties, and that the control-oriented and the original model have similar qualitative and quantitative behavior. In future work, this modeling approach will be the base for the development and analysis of controllers for underwater snake robot locomotion.

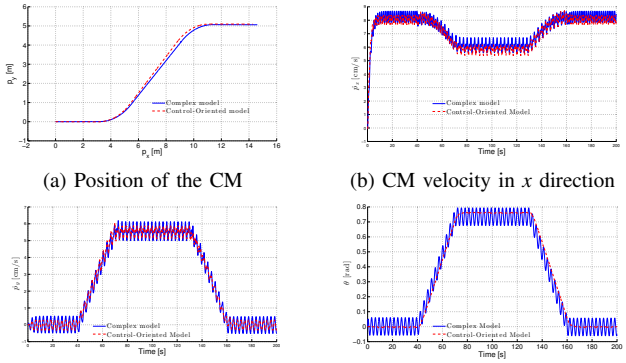

(a) Position of the CM (b) CM velocity in x direction

(c) CM velocity in y direction (d) The orientation

Fig. 6: Simulation results for eel-like motion

REFERENCES

[1] E. Kelasidi, K. Y. Pettersen, J. T. Gravdahl, and P. Liljebäck, "Modelling of underwater snake robots," in *Proc. IEEE International Conference on Robotics and Automation*, 2014 Hong Kong, China, May 31 - June 7 2014. [Online]. Available: https://www.dropbox.com/s/8zg6hk33iarx1j7/ICRA140679.pdf

[2] P. Liljebäck, K. Y. Pettersen, Ø. Stavdahl, and J. T. Gravdahl, *Snake Robots: Modelling, Mechatronics, and Control*. Springer-Verlag, Advances in Industrial Control, 2013.

[3] J. Gray, "Studies in animal locomotion," *Journal of Experimental Biology*, vol. 10, no. 1, pp. 88–104, 1933.

[4] S. Hirose, *Biologically Inspired Robots: Snake-Like Locomotors and Manipulators*. Oxford: Oxford University Press, 1993.

[5] K. McIsaac and J. Ostrowski, "Motion planning for anguilliform locomotion," *IEEE Transactions on Robotics and Automation*, vol. 19, no. 4, pp. 637–625, 2003.

[6] F. Boyer, M. Porez, and W. Khalil, "Macro-continuous computed torque algorithm for a three-dimensional eel-like robot," *IEEE Transactions on Robotics*, vol. 22, no. 4, pp. 763 –775, aug. 2006.

[7] G. Taylor, "Analysis of the swimming of long and narrow animals," *Proceedings of the Royal Society of London. Series A. Mathematical and Physical Sciences*, vol. 214, no. 1117, pp. 158–183, 1952.

[8] M. J. Lighthill, "Large-amplitude elongated-body theory of fish locomotion," *Proceedings of the Royal Society of London. Series B. Biological Sciences*, vol. 179, no. 1055, pp. 125–138, 1971.

[9] J. Chen, W. O. Friesen, and T. Iwasaki, "Mechanisms underlying rhythmic locomotion: bodyfluid interaction in undulatory swimming," *The Journal of Experimental Biology*, vol. 214, no. 4, pp. 561–574, 2011.

[10] A. Wiens and M. Nahon, "Optimally efficient swimming in hyper-redundant mechanisms: control, design, and energy recovery." *Bioinspir Biomim*, vol. 7, no. 4, p. 046016, 2012.

[11] W. Khalil, G. Gallot, and F. Boyer, "Dynamic modeling and simulation of a 3-d serial eel-like robot," *IEEE Transactions on Systems, Man, and Cybernetics, Part C: Applications and Reviews*, vol. 37, no. 6, pp. 1259 –1268, nov. 2007.

[12] J. Blair and T. Iwasaki, "Optimal gaits for mechanical rectifier systems," *IEEE Transactions on Automatic Control*, vol. 56, no. 1, pp. 59–71, 2011.

[13] L. Zhu, Z. Chen, and T. Iwasaki, "Oscillation, orientation, and locomotion of underactuated multilink mechanical systems," *IEEE Transactions on Control Systems Technology*, vol. 21, no. 5, pp. 1537–1548, 2013.

[14] P. Liljeback, K. Pettersen, O. Stavdahl, and J. Gravdahl, "A simplified model of planar snake robot locomotion," in *Proc. IEEE/RSJ International Conference on Intelligent Robots and Systems (IROS)*, 2010, pp. 2868–2875.